Indian J Phys
https://doi.org/10.1007/s12648-026-04107-3

ORIGINAL PAPER

First-principles investigation of K-doped $Rb_7KSn_4H_{16}$ for hydrogen storage: a study of structural, electronic, mechanical, optical, dynamic, and thermal properties

C Kürkçü[1] and C Soykan[2]*

[1]Department of Electronics and Automation, Kırsehir Ahi Evran University, Kirsehir, Turkey

[2]Department of Medical Services and Techniques, Kırsehir Ahi Evran University, Kirsehir, Turkey

Received: 05 February 2026 / Accepted: 16 June 2026

Abstract: The development of efficient and environmentally friendly solid-state hydrogen storage materials remains a major challenge for clean energy technologies. In this study, the structural, electronic, mechanical, optical, vibrational, thermal, and hydrogen storage properties of K-doped $Rb_7KSn_4H_{16}$ were systematically investigated using first-principles density functional theory calculations. The compound was constructed by partial substitution of Rb with K in the parent Rb_2SnH_4 structure to evaluate the effect of alkali-metal doping on hydrogen storage performance and physical properties. The calculated negative formation energy confirms thermodynamic stability, while the absence of imaginary phonon frequencies demonstrates dynamical stability. Electronic structure calculations reveal that $Rb_7KSn_4H_{16}$ is a direct band gap semiconductor with a band gap of 0.722 eV. Mechanical analysis indicates brittle behavior with dominant covalent bonding characteristics. Optical results show enhanced low-energy reflectivity and optical conductivity after K substitution. Thermal calculations indicate robust lattice stability with heat capacity saturation near 140 cal/mol K at elevated temperatures. The compound exhibits a gravimetric hydrogen storage capacity of approximately 2.88 wt%, demonstrating the potential of alkali-metal substitution for tuning complex hydrides. Although this value remains below the current U.S. DOE target for practical applications, the combined thermodynamic, mechanical, and dynamical stability highlights $Rb_7KSn_4H_{16}$ as a promising candidate for future solid-state hydrogen storage research.

Keywords: Hydrogen storage; Electronic; Elastic; Optic; Phonon; Thermal

1. Introduction

Developing clean, efficient, and sustainable energy sources has become a major global challenge due to climate change and the depletion of fossil fuel resources. Among various alternative energy carriers, hydrogen has attracted significant attention because of its high gravimetric energy density (120 MJ/kg) and environmentally friendly nature, producing only water during combustion. However, efficient hydrogen storage, particularly for mobile and portable applications, remains a major obstacle to its widespread utilization in energy systems [1–3].

Hydrogen can be stored through compression, liquefaction, or solid-state storage methods [4]. Among these approaches, solid-state hydrogen storage using metal and complex hydrides has received considerable interest because of its safety, reversibility, and high volumetric and gravimetric storage potential [5]. Consequently, the development of advanced hydrogen storage materials with improved performance has become an important research topic in materials science and renewable energy applications [6–8].

Recent advances in computational materials science, particularly Density Functional Theory (DFT), have enabled the prediction and design of novel hydrogen storage materials with tailored physical properties [9–13]. Alkali and alkaline-earth-metal-based hydrides are especially attractive due to their tunable structural and chemical characteristics through elemental substitution [12, 14–16].

Recent theoretical and experimental studies have demonstrated that compositional engineering can significantly influence the hydrogen storage behavior and multifunctional physical properties of complex hydrides. In

*Corresponding author, E-mail: cengiz.soykan@ahievran.edu.tr

Published online: 05 July 2026

particular, recent first-principles studies by Mubashar and co-authors have provided valuable insight into the effects of structural stability, electronic structure, optical response, and thermodynamic behavior on the hydrogen storage performance of advanced hydride materials [17–23]. Motivated by these developments, the present work investigates the effect of K substitution on the structural, electronic, mechanical, optical, vibrational, and hydrogen storage properties of Rb_2SnH_4-based compounds [24].

Previous studies on Rb_2SnH_4 have reported limitations associated with its thermal stability and hydrogen storage capacity [24]. To overcome these limitations, elemental substitution strategies have been widely employed to modify bonding characteristics, lattice dynamics, and thermodynamic behavior. Such modifications can influence important physical parameters, including Debye temperature and heat capacity, which are closely related to hydrogen adsorption and desorption performance [25].

In this work, we propose a targeted elemental substitution strategy by partially replacing Rb with the lighter K atom to form $Rb_7KSn_4H_{16}$. This substitution is expected to modify the electronic structure, alter vibrational behavior, and influence the thermodynamic stability of the parent compound. Using first-principles DFT calculations, we provide a comprehensive investigation of the structural, electronic, mechanical, optical, vibrational, thermal, and hydrogen storage properties of this compound. To the best of our knowledge, this is the first comprehensive theoretical study of K-doped $Rb_7KSn_4H_{16}$. Furthermore, the results are systematically compared with those of the parent Rb_2SnH_4 compound [24] to clarify the effects of K substitution on the overall hydrogen storage performance and physical properties of the material.

2. Calculation methods

Total energy calculations were performed within the framework of Density Functional Theory (DFT), as implemented in the CASTEP code [26–29]. Using the generalized gradient approximation (GGA) suggested by Perdew, Burke, and Ernzerhof (PBE) [30], the exchange–correlation effects were treated. The geometry optimization of all crystal structures employed pseudopotentials with an energy cutoff of 650 eV for both total energy and stress evaluations.

For periodic crystalline systems, the electronic states are described in reciprocal space, where sampling across the Brillouin zone (BZ) is required. To improve computational efficiency, these quantities are evaluated at a discrete set of k-points within the BZ [31].

The $Rb_7KSn_4H_{16}$ compound was modeled by constructing a $2 \times 1 \times 1$ supercell of $Rb_7KSn_4H_{16}$ and substituting one Rb atom with one K atom. All calculations were performed on this supercell. The interactions between ionic cores and valence electrons were described using ultrasoft pseudopotentials (USP) within the GGA-PBE framework [20]. A Monkhorst–Pack k-point grid of $12 \times 8 \times 6$, optimized for the supercell geometry, was used to sample the reciprocal space [31].

The following valence electron configurations were employed: Rb ($4s^2\ 4p^6\ 5s^1$), Sn ($4d^{10}\ 5s^2\ 5p^2$), K ($3s^2\ 3p^6\ 4s^1$), and H ($1s^1$). Geometric optimization was performed using the BFGS minimization technique with ultrafine accuracy. The convergence criteria were set as: energy change per atom $\leq 1.0 \times 10^{-6}$ eV, maximum Hellmann–Feynman force ≤ 0.01 eV/Å, maximum stress ≤ 0.02 GPa, and maximum atomic displacement $\leq 1.0 \times 10^{-4}$ Å [32].

This setup, utilizing USPs, was also employed for the calculation of elastic constants to ensure consistency in the mechanical properties derived from the optimized geometry [26].

Subsequently, to achieve higher accuracy in the calculation of response properties, single-point energy calculations were performed on the pre-optimized structures using norm-conserving pseudopotentials (NCP). This approach was specifically adopted for determining optical properties (complex dielectric function) and phonon dispersion spectra, as NCPs provide a more accurate description of valence electron wavefunctions required for these calculations [26, 33]. This combined approach enables an effective balance between computational efficiency and numerical accuracy. Ultrasoft pseudopotentials (USP) were employed for structural optimization and elastic calculations to reduce computational cost while maintaining reliable accuracy for the optimized geometry. In contrast, norm-conserving pseudopotentials (NCP) were adopted for optical and phonon calculations because they provide a more accurate description of valence electron wavefunctions, which is essential for response-property calculations. Since all response-property calculations were performed using the same pre-optimized crystal structure, methodological consistency was preserved throughout the study.

The electronic structure was analyzed by calculating the band structure, total density of states (TDOS), and partial density of states (PDOS). Thermal properties, including heat capacity and Debye temperature, were derived from the phonon density of states. Finally, the gravimetric hydrogen storage capacity was evaluated based on the stoichiometry of the optimized compound. The VESTA software was used for visualization of the crystal structure and charge density [34].

3. Results and discussion

3.1. Structural properties

The monoclinic structure of K-doped $Rb_7KSn_4H_{16}$ ($2 \times 1 \times 1$ supercell), which are a member of the space group P2 (International Tables 3, Unique axis b) and reciprocal space group P121, is shown in Fig. 1. There are 28 atoms (H:16, Rb:7, Sn:4, and K:1) in the ($2 \times 1 \times 1$) supercell.

The optimized lattice parameters, volume, and formation energy for K-doped $Rb_7KSn_4H_{16}$ are listed in Table 1. To the best of our knowledge, this is the first theoretical report on this compound, thus no direct comparisons with other studies are available.

In addition, the thermodynamic stability of the P2 (International Table 3, Unique axis b) phase of the K-doped $Rb_7KSn_4H_{16}$ was ascertained by computing the formation energy. Equation 1 calculated a formation energy of −0.020 for this structure.

$$\Delta H_f = \frac{1}{(n_{Rb} + n_{Sn} + n_K + n_{H_2})}[E_{tot}(Rb_7KSn_4H_{16}) - n_{Rb}E_{tot}(Rb) - n_K E_{tot}(K) - n_{Sn}E_{tot}(Sn) - n_{H_2}E_{tot}(H_2)] \quad (1)$$

While E_{Rb}, E_{Sn}, and E_K stand for the total energy of the ground state of the Rb, Sn, and K elements in their bulk forms, respectively, E_{H_2} represents the total energy of the hydrogen molecule. The numbers of Rb, Sn, K, and H atoms in the unit cell are indicated by the symbols n_{Rb}, n_{Sn}, n_K and n_{H_2}. $E_{tot}(Rb_7KSn_4H_{16})$ represents $Rb_7KSn_4H_{16}$'s total energy. The compound has a negative caulated formation energy. This suggests that the structure can be produced experimentally and is thermodynamically stable.

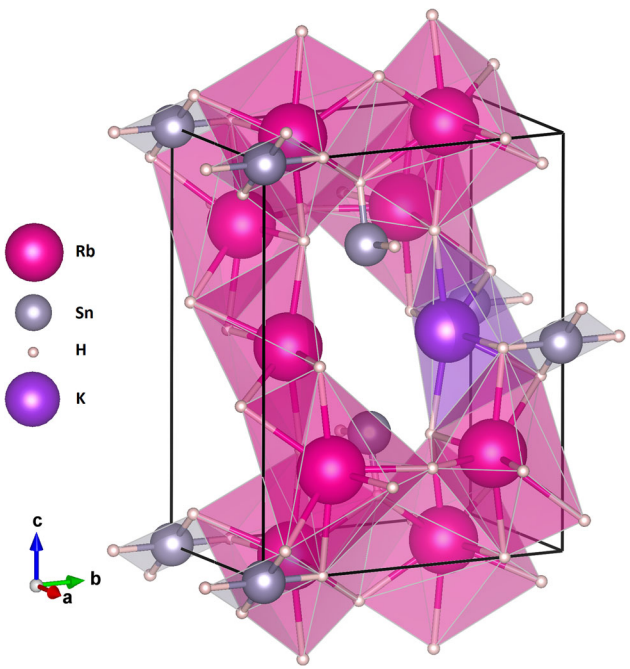

Fig. 1 The crystal structure of K-doped $Rb_7KSn_4H_{16}$ compound

3.2. Electronic properties

The electronic band structure and density of states of K-doped $Rb_7KSn_4H_{16}$ were calculated to elucidate its conductive behavior and orbital interactions. As shown in Fig. 2, the compound exhibits a direct band gap of 0.722 eV at the Γ point, classifying it as a semiconductor. This direct gap suggests potential for optoelectronic applications.

The total and partial density of states (TDOS/PDOS), presented in Fig. 3, provide further insight into the electronic contributions. The valence band, located below the Fermi level (E_F = 0 eV), is primarily composed of Sn-p states in the upper region (0 to −2 eV) and H–s states at lower energies (−2 to −5 eV).

The conduction band, above E_F, is dominated by H–s states near the band edge (0–2 eV), followed by Rb-p states (2–3 eV) and Sn-s states (3–4 eV) at higher energies. This clear separation and character of the states confirm the semiconducting nature of the compound and the covalent character of the bonding, consistent with the mechanical properties.

As shown in Table 2, the Mulliken bond population analysis reveals that the Sn–H interactions possess positive bond populations ranging from 0.33 to 0.81, indicating predominantly covalent bonding with different interaction strengths. In general, shorter Sn–H bond lengths correspond to higher bond populations, suggesting stronger orbital overlap and enhanced bonding interactions. Similar bonding characteristics and electronic interaction trends have also been reported in recent first-principles studies on hydrogen-related functional materials and complex compounds [35–38]. In contrast, the Rb/K–H interactions exhibit near-zero or slightly negative bond populations, reflecting their predominantly ionic character. Furthermore, the negative H–H bond populations confirm the absence of direct H_2-like bonding within the structure. These findings indicate that the structural stability of $Rb_7KSn_4H_{16}$ originates from a mixed covalent–ionic bonding framework dominated by Sn–H interactions.

It should be noted that the calculated band gap was obtained using the GGA-PBE exchange–correlation functional, which is known to underestimate band gap values in semiconducting materials due to its approximate treatment of electron exchange and correlation effects. Therefore, the actual experimental band gap of $Rb_7KSn_4H_{16}$ may be larger than the present theoretical prediction. Nevertheless, GGA-PBE calculations generally provide reliable

qualitative trends for analyzing the electronic structure, bonding characteristics, and comparative effects of elemental substitution. More advanced approaches, such as hybrid functionals (e.g., HSE06), may provide improved quantitative accuracy and could be considered in future investigations.

3.3. Elastic properties

Elastic constants are an extremely important parameter that links the dynamic and mechanical stability of solid materials. It also provides important information about the chemical bonding of atoms with one another in solid materials. In the literature, the elastic constant tensor for monoclinic-type structures consists of thirteen independent elastic constants. These elastic constants are: $C_{11}, C_{22}, C_{33}, C_{44}, C_{55}, C_{66}, C_{12}, C_{13}, C_{15}, C_{23}, C_{25}, C_{35}, C_{46}$ [3]. These elastic constant values are different for seven different crystal systems. The elastic constant values obtained in this study are given in Table 3.

These elastic constants must satisfy the well-known Born stability criteria to understand whether the materials are mechanically stable. The Born criteria determine whether a crystal structure can withstand small stresses without spontaneous failure. The material is mechanically unstable if these criteria are not met; even a small external influence can break it. These criteria also evaluate whether the system can remain energetically stable in the face of small deformations applied to the crystal structure. The Born stability criteria given for monoclinic-type structures are as follows [39]:

$$[C_{11}+C_{22}+C_{33}+2(C_{12}+C_{13}+C_{23})]>0,$$

$$C_{11}>0, C_{22}>0, C_{33}>0, C_{44}>0, C_{55}>0, C_{66}>0,$$

$$\left(C_{33}C_{55}-C_{35}^2\right)>0, C_{44}C_{66}-C_{46}^2>0,$$

$$(C_{22}+C_{33}-2C_{23})>0,$$

$$\left[C_{22}\left(C_{33}C_{55}-C_{35}^2\right)+2\left(C_{23}C_{25}C_{35}-C_{23}^2C_{55}-C_{25}^2C_{33}\right)\right]>0,$$

$$\begin{aligned}&\{2[C_{15}C_{25}(C_{33}C_{12}-C_{13}C_{23})+C_{15}C_{35}(C_{22}C_{13}-C_{12}C_{23})\\&+C_{25}C_{35}(C_{11}C_{23}-C_{12}C_{13})]\\&-\left[C_{15}^2\left(C_{22}C_{33}-C_{23}^2\right)+C_{25}^2\left(C_{11}C_{33}-C_{13}^2\right)+C_{35}^2\left(C_{11}C_{22}-C_{12}^2\right)\right]\\&+C_{55}\left(C_{11}C_{22}C_{33}-C_{11}C_{23}^2-C_{22}C_{13}^2-C_{33}C_{12}^2+2C_{12}C_{13}C_{23}\right)\}>0\end{aligned} \quad (2)$$

Since the elastic constants obtained satisfy the stability criteria given in Eq. 1, the material studied in this structure is mechanically stable.

In the next stage, we will examine the Bulk modulus (B), shear modulus (G), Young's modulus (E), Poisson's ratio v, and Zener anisotropy factory (A) which help us to understand how stiff, elastic, durable, or flexible a material is and can be calculated using the elastic constants obtained and given in Table 4.

The bulk modulus (B), shear modulus (G), Young's modulus (E), and Poisson's ratio (ν) were directly obtained from the CASTEP output. The code employs the Voigt-Reuss-Hill (VRH) averaging scheme to compute these macroscopic mechanical properties for the monoclinic crystal system from the calculated elastic tensor [39].

The mechanical properties of materials are one of the main factors determining their performance in applications. Especially in structural design, it is critical to determine whether the material is ductile or brittle. In this context, the ratio of Bulk modulus (B) to Shear modulus (G), i.e., B/G ratio, is a practical and effective indicator used to predict the ductility and brittleness behavior of materials.

In materials science and engineering, the plastic deformation capacity of a material is directly related to its ductility. Ductile materials deform significantly before fracture, while brittle materials fracture with very little deformation. Quantifying this behavior is of great importance, especially in the design of the next generation of alloys, ceramics, and composite materials. The B/G ratio, proposed by Pugh in 1954 [40], is one of the most widely used criteria for this purpose.

According to Pugh, if the B/G ratio obtained for a material is below 1.75, the material is brittle, and if it is above 1.75, the material has ductile properties. In addition, if this value is above 2.5, it can be said that the material has a very high degree of ductility with plastic deformation

Table 1 The lattice constants (a, b, c in A^0), volume (V in A^3), the formation energy ($\Delta H_f(eV/atom)$), and gravimetric capacity (G_{wt} (%)) of K-doped $Rb_7KSn_4H_{16}$ compound

Material	Lattice constans (A^0) a, b, c	Volume	$\Delta H_f(eV/atom)$	$G_{wt}(\%)$	Reference
$Rb_7KSn_4H_{16}$	5.939, 9.396, 12.569	694.176	− 0.020	2.88	This study

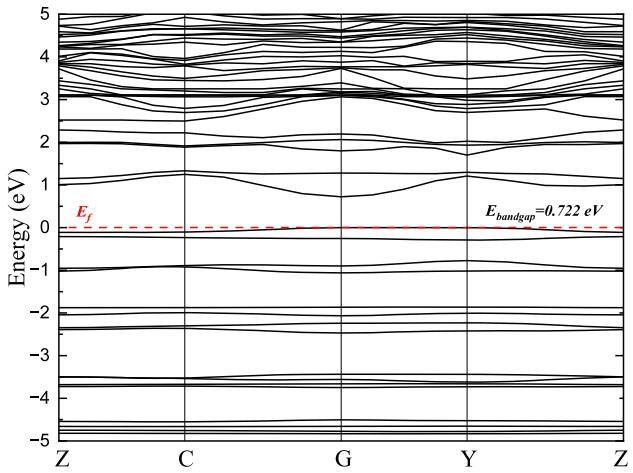

Fig. 2 Electron energy levels along high-symmetry axes for K-doped $Rb_7KSn_4H_{16}$ compound

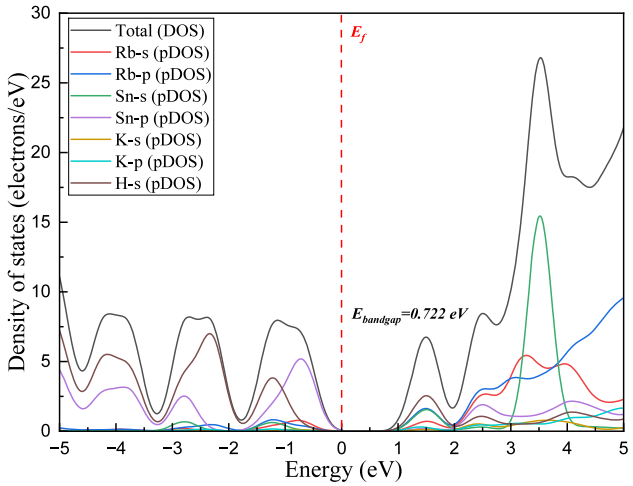

Fig. 3 The total and partial density of states curve for K-doped $Rb_7KSn_4H_{16}$ compound

capability. The material shows brittle qualities since the B/G ratio was found to be 0.934 in this work.

Poisson's ratio provides important information about the volume change and strain behavior of a material under load. When a material elongates during elastic deformation, the bonds between the atoms open while the sides contract. This behavior is studied by Poisson's ratio. Should the Poisson's ratio be approximately 0.1, the atoms comprising the substance create covalent links with one another. Should this ratio be approximately 0.25, they create ionic bonds. Should it be about 0.5, they create metallic connections, which are weaker. The atoms are covalently linked to one another since the Poisson's ratio value acquired in this work is 0.106.

Most elastic properties of materials with crystalline structures are modeled assuming that they are isotropic. However, especially in materials with crystalline structures such as single crystal structures, ceramics, metals, and intermetallic compounds, elastic properties can vary depending on the crystal orientation. This is defined as elastic anisotropy. One of the most common parameters used to quantitatively evaluate this difference is the Zener anisotropy ratio [41]. If A = 1, the material behaves elastically isotropically. This implies that the structure exhibits direction-independent mechanical properties. If $A \neq 1$, the material is anisotropic, meaning that it gives different elastic responses in different directions. The further A is from 1, the greater the anisotropy.

3.4. Optical properties

The optical properties of K-doped $Rb_7KSn_4H_{16}$ were investigated through the complex dielectric function, $\varepsilon(\omega) = \varepsilon_1(\omega) + i\varepsilon_2(\omega)$, which provides essential information about the interaction between the material and electromagnetic radiation. Based on this function, optical parameters such as optical conductivity, reflectivity, and absorption coefficient were calculated.

Figure 4 displays the energy-dependent real (ε_1) and imaginary (ε_2) parts of the dielectric function. The real part, ε_1, which is associated with polarization and refractive behavior, exhibits a significant static dielectric constant [$\varepsilon_1(0)$] and a prominent peak at approximately 1.24 eV. This low-energy feature indicates strong electronic polarization in the infrared region. Subsequently, ε_1 decreases to negative values in the intermediate energy range ($\sim$ 5–15 eV), indicating metallic-like reflective behavior. The plasma resonance frequency, identified by the zero-crossing of ε_1, is observed around 10.5 eV.

The imaginary part, ε_2, which represents optical absorption, reveals the onset of direct electronic transitions near the fundamental band gap ($\sim$ 0.72 eV). The main absorption peaks observed at 3.93 eV and 5.76 eV originate from transitions between the valence and conduction bands, consistent with the PDOS results presented in Fig. 3. The overall dielectric response confirms the semiconducting character of the compound, while the pronounced low-energy features indicate that K substitution significantly modifies the electronic structure compared to the parent Rb_2SnH_4 compound [24].

The imaginary part of the dielectric function, $\varepsilon_2(\omega)$, shown in Fig. 4, provides insight into the optical absorption and interband transitions of $Rb_7KSn_4H_{16}$. The onset of ε_2 around 0.72 eV corresponds to the fundamental direct band gap, consistent with the electronic structure calculations. The prominent peaks at 3.93 eV and 5.76 eV originate from major interband transitions between the valence and conduction bands, indicating strong optical absorption in this energy region. These features are also consistent with

Table 2 Representative Mulliken bond populations and bond lengths for $Rb_7KSn_4H_{16}$

Bond	Bond population	Bond length (A^0)	Bond character
Sn–H	0.81	1.786	Strong covalent
Sn–H	0.65	1.870	Moderate covalent
Sn–H	0.33	2.156	Weak covalent
H–H	− 0.15 to − 0.11	2.600	Non-bonding/repulsive
Rb–H	0.00	2.902–2.950	Predominantly ionic
K–H	0.00	2.923	Predominantly ionic

the PDOS results presented in Fig. 3. The subsequent minimum in ε_2 around 13.12 eV indicates reduced optical loss and coincides with the energy range where $\varepsilon_1(\omega)$ becomes positive again. At higher energies, the features above 15 eV, including the peak at 19.69 eV, are attributed to deeper electronic excitations. Finally, the convergence of $\varepsilon_2(\omega)$ toward zero beyond 27 eV suggests that the material becomes nearly transparent at energies above the plasmon frequency.

A comparative analysis with the parent compound Rb_2SnH_4 [24] reveals that K substitution in $Rb_7KSn_4H_{16}$ enhances the low-energy dielectric response. This is evidenced by the increased intensity of the first peak in $\varepsilon_1(\omega)$ below 3 eV, indicating stronger electronic polarization in the infrared region. While the overall behavior of $\varepsilon(\omega)$ in the mid- and high-energy regions remains largely unchanged, the low-energy modification highlights the effectiveness of elemental substitution in tuning the optoelectronic response of the material.

The frequency-dependent optical conductivity, $\sigma(\omega)$, of $Rb_7KSn_4H_{16}$ is presented in Fig. 5. The real part of the optical conductivity, $\sigma_1(\omega)$, begins to increase near the fundamental band gap ($\sim$ 0.72 eV), consistent with the onset of optical absorption. The spectrum exhibits two prominent peaks. The first major peak, located at 5.93 eV with an intensity of 2.44 (1/fs), originates from dominant interband electronic transitions and corresponds to the main absorption region observed in the $\varepsilon_2(\omega)$ spectrum (Fig. 4). A second broader and more intense peak appears at 19.81 eV with an intensity of 3.06 (1/fs), which is associated with higher-energy electronic excitations.

The overall shape of the optical conductivity spectrum is consistent with the dielectric function analysis. The gradual decrease in $\sigma_1(\omega)$ beyond the main peaks indicates a reduction in interband electronic transitions at higher energies. Furthermore, the convergence of the optical conductivity toward zero above approximately 29 eV suggests the disappearance of significant photo-response in this energy region.

The optical reflectivity spectrum, $R(\omega)$, of $Rb_7KSn_4H_{16}$ is displayed in Fig. 6. The material exhibits relatively high reflectivity in the low-energy region (below $\sim$ 3 eV), consistent with the enhanced low-energy dielectric response observed in $\varepsilon_1(\omega)$. This behavior is associated with the semiconducting nature of the compound and its relatively low optical absorption in this energy range.

The reflectivity spectrum exhibits features consistent with the electronic transitions observed in the $\varepsilon_2(\omega)$ and $\sigma_1(\omega)$ spectra. In the intermediate energy region, the reflectivity decreases due to enhanced optical absorption. At higher energies, beyond approximately 36 eV, the reflectivity approaches zero, indicating that the material becomes nearly transparent to high-energy photons.

The frequency-dependent optical absorption coefficient, $\alpha(\omega)$, of $Rb_7KSn_4H_{16}$ is presented in Fig. 7. The absorption spectrum exhibits two primary maxima at 6.43 eV and 21.33 eV, corresponding to the major interband transitions identified in the $\varepsilon_2(\omega)$ and $\sigma_1(\omega)$ spectra. A region of reduced absorption is observed around 13.24 eV, which coincides with a similar decrease in the optical conductivity spectrum. This behavior indicates consistency among the calculated optical properties.

The absorption edge appears near the fundamental band gap ($\sim$ 0.72 eV), confirming the semiconducting nature of the compound. At higher energies (above $\sim$ 29 eV), the absorption coefficient approaches zero, indicating that the material becomes nearly transparent to high-energy photons.

3.5. Vibrational properties

The dynamical stability of $Rb_7KSn_4H_{16}$ was assessed by calculating its phonon dispersion spectrum along high-symmetry directions in the Brillouin zone (Z-C-Γ-Y-Z), as presented in Fig. 8. The absence of any imaginary frequencies (soft modes) across the entire Brillouin zone confirms that the compound is dynamically stable. This is a crucial prerequisite for its practical synthesis and application.

Table 3 The independent elastic constants (C_{ij} in GPa) for K-doped $Rb_7KSn_4H_{16}$ compound

Material	C_{11}	C_{12}	C_{13}	C_{15}	C_{23}	C_{25}	C_{35}	Functional
$Rb_7KSn_4H_{16}$	13.299	2.422	1.326	2.391	23.419	0.097	2.390	GGA-PBE present
	C_{46}	C_{22}	C_{33}	C_{44}	C_{55}	C_{66}		
	0.714	10.810	26.477	8.597	5.853	5.996		

Table 4 The calculated mechanical properties (Bulk modulus B, Shear modulus G, Young's modulus E in GPa), B/G ratio, Zener anisotropy factor (A), Poisson's ratio (ν) for K-doped $Rb_7KSn_4H_{16}$ compound

Material (GPa)	B	G	E	B/G	A	υ	Functional
$Rb_7KSn_4H_{16}$	10.493	11.229	24.831	0.934	1.581	0.106	GGA-PBE present

The unit cell of $Rb_7KSn_4H_{16}$ contains 28 atoms, resulting in a total of 84 phonon branches (3N, where N = 28). As expected, three acoustic branches are visible in the low-frequency region, originating from the Γ point, while the remaining 81 branches are optical modes. The significant gap between the low-frequency acoustic modes and the higher-frequency optical modes is indicative of the mass difference between the heavy metal atoms (Rb, K, Sn) and the light hydrogen atoms. The optical modes above approximately 15 THz are predominantly associated with hydrogen vibrations, which are critical for hydrogen storage properties as they relate to the stability and dynamics of the hydrogen bonds within the structure.

3.6. Thermal properties

The thermal properties of $Rb_7KSn_4H_{16}$, derived from the phonon density of states, are presented in Figs. 9 and 10. The temperature dependence of the heat capacity (C_V) follows the characteristic trend for solids, as described by the Debye model [42–45]. At very low temperatures ($T < 100$ K), C_V exhibits a T^3 dependence. It then increases rapidly and approaches a near-constant value of approximately 140 cal/mol K at high temperatures, in accordance with the Dulong-Petit law [42–44].

The incorporation of the lighter K atom in place of Rb is expected to influence the vibrational spectrum, leading to a modification of the thermal properties compared to the parent compound. This is reflected in the calculated Debye temperature (Θ_D), shown in Fig. 10. The value of Θ_D, which is a measure of the lattice stiffness and the maximum phonon frequency, stabilizes at higher temperatures, indicating robust thermal stability of the crystal lattice over a wide temperature range [45]. This thermal stability is a desirable property for hydrogen storage materials, as it suggests that the material can maintain its structural integrity during repeated hydrogen adsorption and desorption cycles, which involve temperature variations.

3.7. Hydrogen storage properties

The hydrogen storage potential of K-doped $Rb_7KSn_4H_{16}$ was evaluated based on its stoichiometry and the calculated physical properties discussed in previous sections. The gravimetric hydrogen storage capacity was calculated to be approximately 2.88 wt%, according to the standard gravimetric capacity equation [46]. This value is competitive for complex hydrides and meets one of the preliminary benchmarks for practical solid-state hydrogen storage systems.

This storage capacity, coupled with the material's fundamental properties, underscores its promise. The compound is thermodynamically stable (negative formation energy), mechanically stable (satisfies Born criteria), and dynamically stable (no soft phonon modes). Crucially, the thermal analysis indicates high thermal stability over a wide temperature range (Figs. 9 and 10). A stable Debye temperature (Θ_D) profile at elevated temperatures suggests that the crystal lattice can withstand thermal stresses, which is essential for the structural integrity of a material undergoing repeated hydrogen adsorption and desorption cycles.

Furthermore, the constituent elements (K, Rb, Sn) are generally considered to have low environmental toxicity. Unlike some other hydrogen storage materials, such as NH_3BH_3 which releases toxic ammonia upon decomposition, $Rb_7KSn_4H_{16}$ is not expected to produce highly harmful byproducts during hydrogen release. This combination of a respectable theoretical capacity, multifaceted stability, and a relatively benign environmental profile positions K-doped $Rb_7KSn_4H_{16}$ as a promising and sustainable candidate for further investigation in solid-state

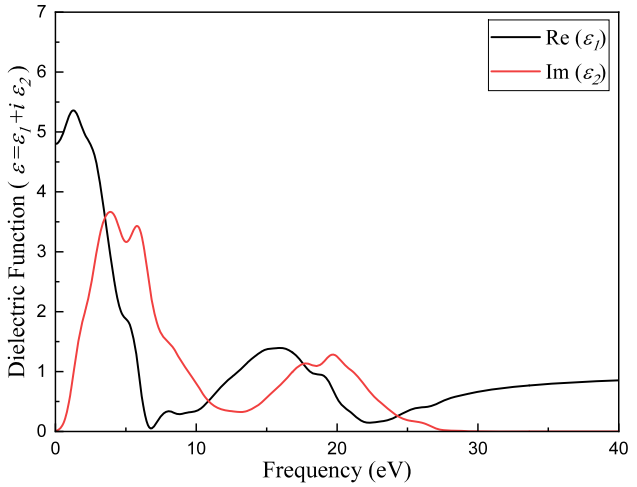

Fig. 4 The optical dielectric function for K-doped $Rb_7KSn_4H_{16}$ compound

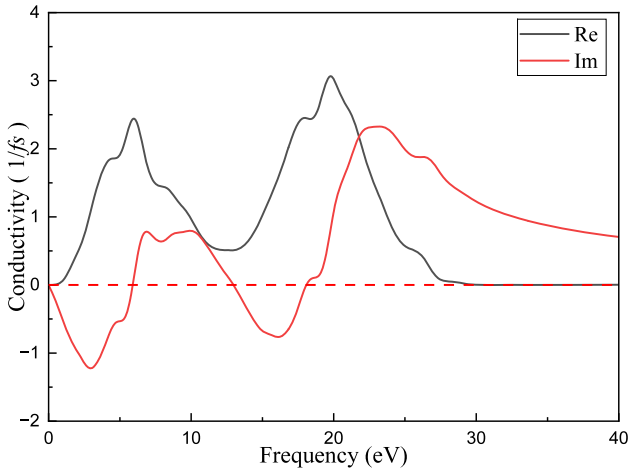

Fig. 5 The optical conductivity (1/fs) for K-doped $Rb_7KSn_4H_{16}$ compound

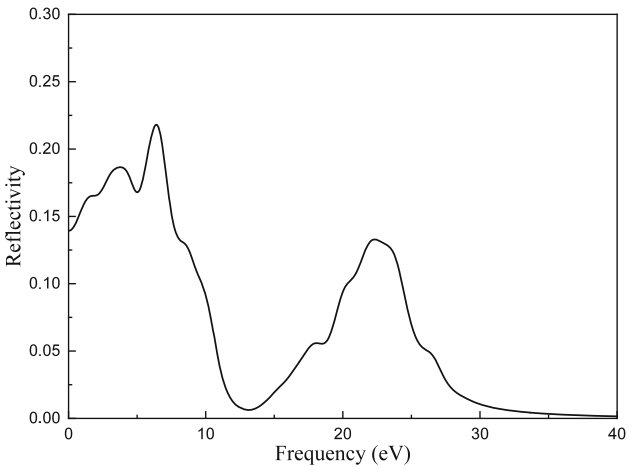

Fig. 6 The optical reflectivity for K-doped $Rb_7KSn_4H_{16}$ compound

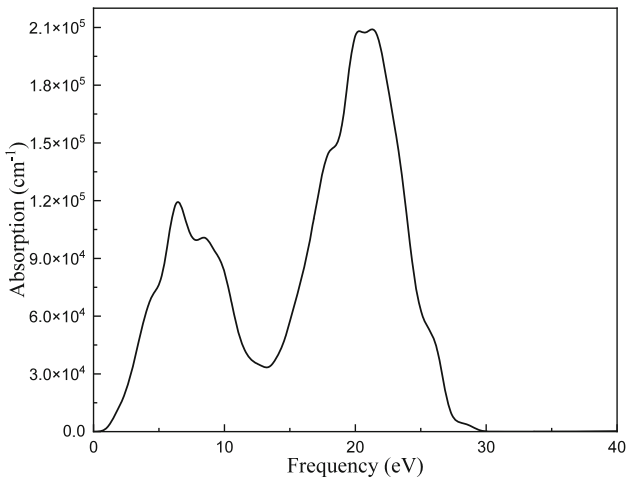

Fig. 7 The optical absorption (cm^{-1}) for K-doped $Rb_7KSn_4H_{16}$ compound

hydrogen storage applications, such as in fuel cells and renewable energy storage systems.

Although the calculated gravimetric hydrogen storage capacity of $Rb_7KSn_4H_{16}$ (2.88 wt%) demonstrates the potential of alkali-metal substitution for tuning complex hydrides, this value remains below the current U.S. Department of Energy (DOE) target (∼ 5.5 wt%) for practical onboard hydrogen storage systems. In addition, important practical parameters such as hydrogen desorption temperature, adsorption/desorption kinetics, reversibility, and cycling stability were not evaluated in the present theoretical study. Therefore, further experimental and advanced computational investigations are necessary to fully assess the practical applicability of this material for real hydrogen storage technologies.

For a more comprehensive assessment, the hydrogen storage capacity of $Rb_7KSn_4H_{16}$ (2.88 wt%) can be compared with both the U.S. DOE target (∼ 5.5 wt%) and other representative complex hydrides reported in the literature. For instance, several alkali-metal-based hydrides and doped systems typically exhibit hydrogen storage capacities in the range of 1–5 wt%, depending on their structural and chemical composition. Although the present compound does not yet reach the DOE target, its performance is comparable to many recently reported theoretical hydride systems, particularly those investigated via first-principles calculations. When combined with its thermodynamic, mechanical, and dynamical stability, this comparison suggests that $Rb_7KSn_4H_{16}$ may serve as a useful reference system for further compositional engineering aimed at improving hydrogen storage performance.

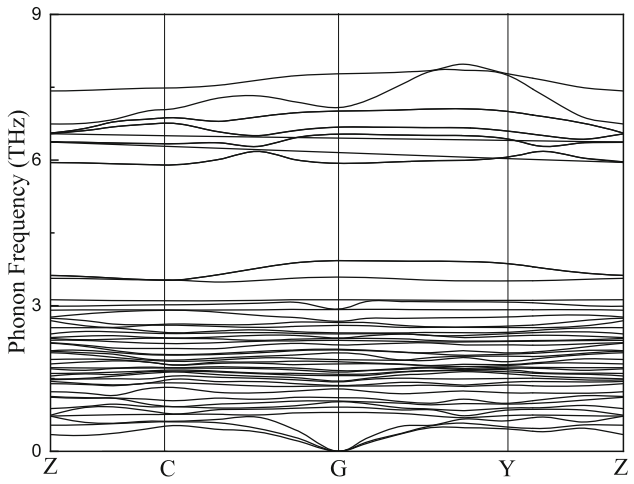

Fig. 8 Variation of phonon frequencies along high-symmetry points for K-doped $Rb_7KSn_4H_{16}$ compound

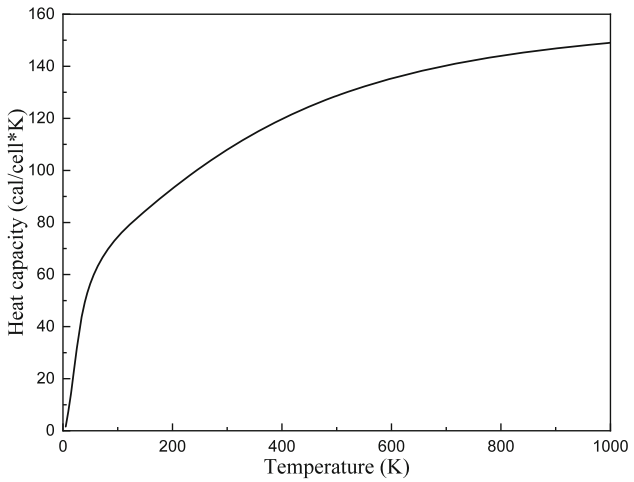

Fig. 9 The heat capacity curve for K-doped $Rb_7KSn_4H_{16}$ compound

To provide a clearer perspective on the performance of the present compound, a comparative summary of $Rb_7KSn_4H_{16}$ with representative hydrogen storage materials is presented in Table 5. The comparison includes key parameters such as hydrogen storage capacity, electronic band gap, and stability characteristics.

As seen in Table 5, the hydrogen storage capacity of $Rb_7KSn_4H_{16}$ (2.88 wt%) is comparable to several reported complex hydrides, including Rb_2SnH_4 and Mg-based hydrides, while remaining lower than highly optimized systems such as certain $XGaH_5$ (X=Ca, Mg) compounds. Despite this moderate storage capacity, $Rb_7KSn_4H_{16}$ demonstrates a balanced combination of thermodynamic, mechanical, and dynamical stability, which is not always simultaneously achieved in many higher-capacity hydride systems. In addition, its relatively narrow band gap (0.722 eV) suggests favorable electronic tunability

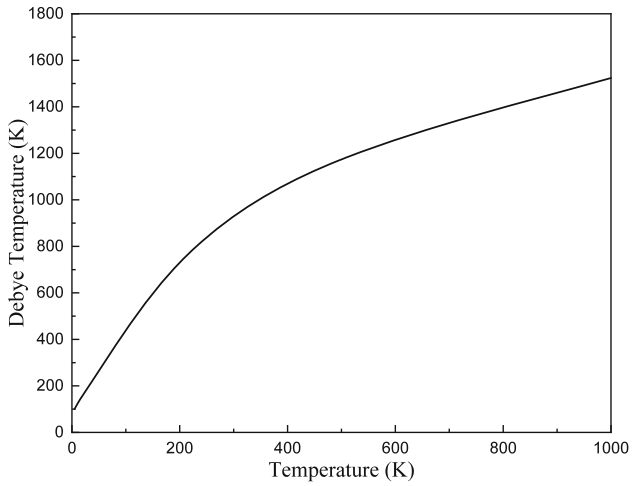

Fig. 10 The Debye temperature curve for K-doped $Rb_7KSn_4H_{16}$ compound

compared to wider-gap hydrides such as $XGaH_5$ compounds. Overall, this comparison indicates that while the hydrogen storage capacity is not among the highest reported values, the multifunctional stability and consistent physical properties position $Rb_7KSn_4H_{16}$ as a structurally robust candidate for further materials design strategies.

4. Conclusions

In this study, we presented a comprehensive first-principles investigation of the structural, electronic, mechanical, optical, dynamic, thermal, and hydrogen storage properties of the K-doped rubidium tin hydride, $Rb_7KSn_4H_{16}$.

Our calculations confirm that the compound is thermodynamically stable, as evidenced by its negative formation energy. Electronic structure analysis reveals a direct band gap of 0.722 eV, characteristic of a semiconductor. Mechanically, the compound is stable according to the Born criteria for monoclinic crystals and exhibits brittle behavior with predominantly covalent bonding, as indicated by a Pugh's ratio (B/G) of 0.934 and a Poisson's ratio of 0.106. The optical properties demonstrate strong low-energy features, including high reflectivity and conductivity, suggesting potential for optoelectronic applications in the infrared regime.

Crucially, the compound's dynamic stability is confirmed by the absence of imaginary frequencies in its phonon dispersion spectrum. Thermal property calculations indicate a high heat capacity, saturating at approximately 140 cal/mol K, and a stable Debye temperature profile, both signifying robust thermal stability over a wide temperature range. This is a key attribute for a material intended for cyclic hydrogen storage and release operations.

Table 5 Comparison of $Rb_7KSn_4H_{16}$ with selected hydrogen storage materials

Material	$G_{wt}(\%)$	Band gap (eV)	Stability	Method	References
$Rb_7KSn_4H_{16}$	2.88	0.722	Stable	GGA-PBE	This study
Rb_2SnH_4	2.77	0.455	Stable	GGA-PBE	[24]
Mg_2NiH_4	3.6	1.348	Stable	GGA-PBE	[8, 47]
Mg_2RuH_4		0.877	Stable	GGA-PBE	[8]
$XGaH_5$ (X=Ba, Ca, Mg)	2.38, 4.4, 5.1	3.08, 4.05, 3.61	Stable	GGA-PBE	[3]

Most significantly, the compound exhibits a gravimetric hydrogen storage capacity of 2.88 wt%, demonstrating the influence of alkali-metal substitution on tuning the properties of complex hydrides. Although this value remains below the current U.S. DOE target for practical hydrogen storage applications, the combined thermodynamic, mechanical, and dynamical stability of K-doped $Rb_7KSn_4H_{16}$ suggests that it may serve as a useful candidate for further theoretical and experimental investigations in solid-state hydrogen storage research.

Acknowledgements This study was supported by the Kırşehir Ahi Evran University under Scientific Research Project No: TBY.A1.24.001.

Author contributions Cengiz Soykan: Supervision, Writing—review & editing, Writing—original draft, Methodology, Investigation. **Cihan Kurkcu**: Writing—review & editing, Writing—original draft, Methodology, Investigation.

Data availability The data that support the findings of this study are available from the corresponding author, Cengiz Soykan, upon reasonable request.

Declarations

Conflict of interest The authors declare that they have no known competing financial interests or personal relationships that could have appeared to influence the work reported in this paper.

Declaration of generative AI and AI-assisted technologies in the writing process During the preparation of this work, the author(s) used an artificial intelligence tool to improve the language and readability of the study. After using this tool/service, the author(s) reviewed and edited the content as needed and take(s) full responsibility for the content of the publication.

References

[1] M M H Bhuiyan and Z Siddique *Int. J. Hydrog. Energy* **102** 1026 (2025)
[2] A M Sadeq, R Z Homod, A K Hussein, H Togun, A Mahmoodi, H F Isleem, A R Patil and A H Moghaddam *Sci. Total Environ.* 173622 (2024)
[3] Ç Yamçıçıer and C Kürkçü *Int. J. Hydrog. Energy* **81** 391 (2024)
[4] S Z Al Ghafri, S Munro, U Cardella, T Funke, W Notardonato, J M Trusler, J Leachman, R Span, S Kamiya and G Pearce *Energy Environ. Sci.* **15** 2690 (2022)
[5] N A A Rusman and M Dahari *Int. J. Hydrog. Energy* **41** 12108 (2016)
[6] A S Mehr, A D Phillips, M P Brandon, M T Pryce and J G Carton *Int. J. Hydrog. Energy* **70** 786 (2024)
[7] K Yvon and G Renaudin *Encycl. Inorg. Chem.* (2006)
[8] Ç Yamçıçıer and C Kürkçü *J. Energy Storage* **84** 110883 (2024)
[9] X Yang, Y Li, Y Liu, Q Li, T Yang and H Jia *Energies* **17** 3591 (2024)
[10] A Jain, Y Shin and K A Persson *Nat. Rev. Mater.* **1** 1 (2016)
[11] C Soykan *Phys. Chem. Chem. Phys.* **28** 7465 (2026)
[12] C Soykan and H Gocmez *Phys. B Condens. Matter* **608** 412897 (2021)
[13] C Soykan and C Kürkçü *Int. J. Hydrog. Energy* **202** 153033 (2026)
[14] T He, H Cao and P Chen *Acc. Mater. Res.* **2** 726 (2021)
[15] M A Rahman and A A Hossain *Int. J. Hydrog. Energy* **97** 457 (2025)
[16] C Kurkcu, S Al and C Yamcicier *Eur. Phys. J. B* **95** 180 (2022)
[17] M Ali, Z Bibi and T Akhter *Int. J. Hydrog. Energy* **202** 153054 (2026)
[18] M Ali, Z Bibi, A F Khan, I Taj and M Jawad *Inorg. Chem. Commun.* **181** 115186 (2025)
[19] M Ali, Z Bibi, M Mubashir, M W Younis, U Afzal and A Elmarghany *ChemistrySelect* **9** e202304582 (2024)
[20] M Ali, Z Bibi, M W Younis, K Majeed, U Afzal, S Khan, N H Alotaibi and M Mubashir *Int. J. Hydrog. Energy* **70** 579 (2024)
[21] M Ali, Z Bibi, M Awais, M W Younis and N Sfina *Int. J. Hydrog. Energy* **64** 329 (2024)
[22] M Ali, M Raheel and Z Bibi *J. Hydrog. Energy* **128** 749 (2025)
[23] Z Bibi, M Ali, M Yousaf and A Zafar *J. Eng. Sci. Technol. Trends* **1** 100 (2024)
[24] C Soykan and C Kürkçü *J. Phys. Chem. Solids* 112618 (2025)
[25] M Komeili, H Arabi, R V Yusupov, S R Ghorbani, F G Vagizov and F Pourarian *Int. J. Hydrog. Energy* **46** 19060 (2021)
[26] S J Clark, M D Segall, C J Pickard, P J Hasnip, M I Probert, K Refson and M C Payne *Z. Für Krist.-Cryst. Mater.* **220** 567 (2005)
[27] G Kresse and J Furthmüller *Comput. Mater. Sci.* **6** 15 (1996)
[28] G Kresse and J Furthmüller *Phys. Rev. B* **54** 11169 (1996)
[29] G Kresse and J Hafner *J. Phys. Condens. Matter* **6** 8245 (1994)
[30] J P Perdew, K Burke and M Ernzerhof *Phys. Rev. Lett.* **77** 3865 (1996)
[31] H J Monkhorst and J D Pack *Phys. Rev. B* **13** 5188 (1976)
[32] T H Fischer and J Almlof *J. Phys. Chem.* **96** 9768 (1992)
[33] K Lejaeghere, V Van Speybroeck, G Van Oost, and S Cottenier *Crit. Rev. Solid State Mater. Sci.* **39** 1 (2013)
[34] K Momma and F Izumi *Appl. Crystallogr.* **41** 653 (2008)
[35] M Ali, Z Bibi, M W Younis, M Mubashir, M Iqbal, M Usman Ali and M Asif Iqbal *Sol. Energy 267* 112199 (2024)
[36] M Mubashir, Z Bibi, M Ali, M Muzamil, U Afzal and M D Albaqami *Phys. B Condens. Matter* **685** 415986 (2024)
[37] M Ali, Z Bibi, M W Younis and M Asif Iqbal *Inorg. Chem. Commun.* **160** 111891 (2024)

[38] M Ali, Z Bibi, M W Younis, H Huang, M Raheel, U Afzal, R A Alshgari and S Mohammad *J. Inorg. Organomet. Polym. Mater.* **35** 3313 (2025)
[39] F Mouhat and F-X Coudert *Phys. Rev. B* **90** 224104 (2014)
[40] S F Pugh *Lond. Edinb. Dublin Philos. Mag. J. Sci.* **45** 823 (1954)
[41] C M Kube *AIP Adv.* **6** (2016)
[42] S Baroni, S De Gironcoli, A Dal Corso and P Giannozzi *Rev. Mod. Phys.* **73** 515 (2001)
[43] M C Warren and G J Ackland *Phys. Chem. Miner.* **23** 107 (1996)
[44] M C Warren, G J Ackland, B B Karki and S J Clark *Mineral. Mag.* **62** 585 (1998)
[45] N W Ashcroft and N D Mermin *N. Y.* (1976)
[46] A Züttel *Mater. Today* **6** 24 (2003)
[47] J J Reilly and R H Wiswall *Inorg. Chem.* **7** 2254 (1968)